

Experimental optical phase measurement at the exact Heisenberg limit

Shakib Daryanoosh,¹ Sergei Slussarenko,¹ Dominic W. Berry,² Howard M. Wiseman,^{1,*} and Geoff J. Pryde^{1,†}

¹*Centre for Quantum Dynamics and Centre for Quantum Computation and Communication Technology, Griffith University, Brisbane, Queensland 4111, Australia*

²*Department of Physics and Astronomy, Macquarie University, Sydney NSW 2113, Australia*

The use of quantum resources can provide measurement precision beyond the shot noise limit (SNL). The task of *ab initio* optical phase measurement¹—the estimation of a completely unknown phase—has been experimentally demonstrated with precision beyond the SNL, and even scaling like the ultimate bound, the Heisenberg limit (HL)², but with an overhead factor. However, existing approaches have not been able—even in principle—to achieve the best possible precision, saturating the HL exactly. Here we demonstrate a scheme to achieve true HL phase measurement, using a combination of three techniques: entanglement, multiple samplings of the phase shift, and adaptive measurement. Our experimental demonstration of the scheme, with photonic qubits and $N = 3$ photon-passes, achieves a precision that is within 4% of the HL, surpassing the best precision theoretically achievable with simpler techniques. This work represents a fundamental achievement of the ultimate limits of metrology, and the scheme can be extended to higher N and other physical systems.

Precise measurement is at the heart of science and technology³. An important fundamental concern is how to achieve the best precision in measuring a physical quantity, relative to the resources of the probe system. As physical resources are fundamentally quantised, it is quantum physics that determines the ultimate precision that can be achieved. Correlated quantum resources⁴ such as entangled states can provide an enhancement over independent use of quantum systems in measurement.

Quantum-enhanced optical phase estimation promises improvements in all measurement tasks for which interferometry is presently used^{5,6}. Such optical quantum metrology can be divided into two distinct tasks. In phase *sensing*, the goal is to determine small deviations in a phase about an already well-known value—a very specific situation. The use of maximally-path-entangled NOON states^{7,8} can, in principle, provide optimal sensitivity for this task^{9–11}. The more challenging task is phase *measurement*, sometimes called *ab initio* phase measurement, in which the aim is to determine an unknown phase ϕ with no prior information about its value. In this case, the use of multiple passes of the optical phase shift and adaptive quantum measurement², or entanglement and adaptive quantum measurement¹², have been shown to be capable of surpassing the shot noise limit (SNL), $V^{\text{SNL}} = 1/N$ (for large N). The SNL represents the minimum variance achievable with a definite number N of independent samples of the phase shift by a photon. By making correlated samples of the phase shift, these schemes^{2,12,13} can achieve an asymptotic variance $V = (C\pi/N)^2$. This is proportional to, but with a constant overhead $C > 1$ over, the ultimate limit (the Heisenberg limit, HL) of $(\pi/N)^2$ for the asymptotic *ab initio* task. To be precise, in terms of Holevo’s variance

measure^{14,15}, the exact HL for any value of N is

$$V^{\text{HL}} = \tan^2[\pi/(N+2)]. \quad (1)$$

Phase measurement schemes are not limited to optics: equivalent techniques have also used phase shifts of superposition states of single-NV-centre measurements induced by magnetic fields^{16,17}, for example.

Here we demonstrate a technique to address this outstanding, fundamental question of quantum metrology: how to measure phase at the *exact* HL? We show a concrete way to implement the conceptual scheme previously proposed in theory¹⁵, and implement it experimentally. The basic concept of optical phase measurement with photons is shown in Fig. 1a. The phase to be measured is inserted in one path of an interferometer; the other path is the reference arm. In the language of quantum information, a photon incident on the first beam splitter (BS) is represented by the logical state $|0\rangle$. The action of the BS is modelled by a Hadamard gate $H|0\rangle = (|0\rangle + |1\rangle)/\sqrt{2}$. The unknown phase shift applied on path $|1\rangle$ is represented by the unitary gate $U(\phi) = \exp(i\phi|1\rangle\langle 1|)$. The last BS prior to detection stages maps the logical Z basis onto the X basis.

A more general protocol may include more sophisticated techniques. The relevant constituents are: 1. the quantum state of the light in the interferometer paths; 2. the possibility of multiple coherent samplings of the phase shift by some photons; and 3. the detection strategy. For example, Fig. 1b generalises the basic single photon interferometer to include $p \geq 1$ applications of $U(\phi)$ and a classically controllable phase, described by $R(\theta) \equiv \exp(i\theta|0\rangle\langle 0|)$, on reference path $|0\rangle$. We can also depict this interferometer following the quantum circuit convention, as in Fig. 1c.

For *ab initio* phase measurement with N photons and no multipassing ($p = 1$), it is known theoretically that the HL can be achieved by preparing a path-entangled state^{18,19} and implementing an entangling detection scheme²⁰. The problem is that both of these steps

* h.wiseman@griffith.edu.au

† g.pryde@griffith.edu.au

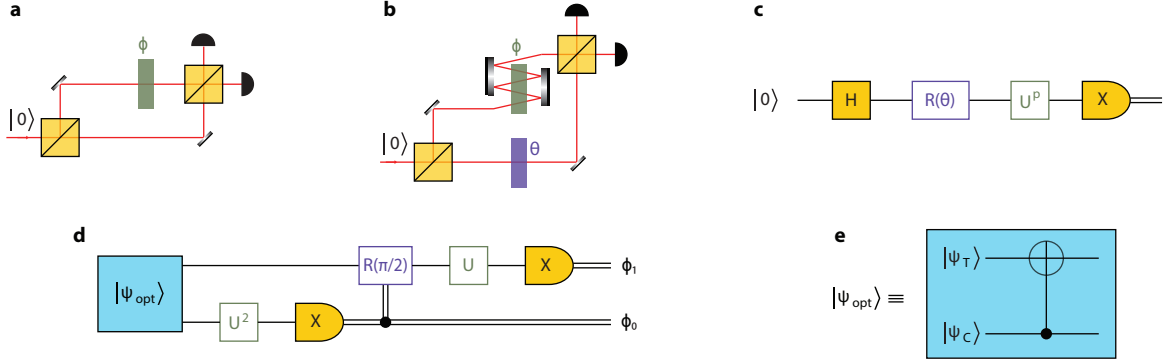


FIG. 1. **Optical phase measurement concept.** **a**, Basic interferometric phase estimation setup. **b**, Conceptual scheme of an advanced interferometer that includes multiple (p) passes of the phase shift ϕ and a controllable phase θ in the reference arm. **c**, Quantum circuit representation of the interferometer shown in **b**. **d**, Quantum circuit for Heisenberg-limited interferometric phase estimation with $N = 3$ resources. The protocol is extensible to higher N , in principle¹⁵. **e**, Quantum circuit for the preparation of the optimal state $|\psi_{\text{opt}}\rangle$, Eq. (2), using a CNOT gate with control and target qubits prepared in $|\psi_C\rangle$ and $|\psi_T\rangle$, respectively.

are very difficult to do. An alternate way¹⁵ to achieving the HL uses entanglement across multiple spatio-temporal modes, and multiple applications p of the phase gate, combined with the inverse quantum Fourier transform (IQFT) for the measurement. While the IQFT is also an entangling operation, it has been known for some time²¹ that, in this “phase estimation algorithm” (PEA)²², it can be replaced by an adaptive measurement scheme³, where individual photons are measured one by one, with the reference phase adjusted after each measurement. This replacement requires the photons in the entangled state to be spread out in time, but suffers no penalty in measurement precision.

Here, we show the practicality of combining entanglement, multipassing and adaptive measurement to achieve the HL. Our Heisenberg-limited interferometric phase estimation algorithm (HPEA)¹⁵ is illustrated in Fig. 1d. This protocol is based on the standard PEA such that using $K + 1$ qubits yields an estimate ϕ_{est} of the true phase ϕ with $K + 1$ bits of precision²². It involves application of the phase gate $N = 2^{K+1} - 1$ times, with the number of applications being $p = 2^K, 2^{K-1}, \dots, 2^0$ on each successive qubit (photon). Our particular demonstration is an instance of a ($K + 1 =$) 2-photon superposition state¹⁵ that may be used to perform a protocol with $N = 2^{K+1} - 1 = 3$ resources, achieving a variance for *ab initio* phase estimation of exactly V^{HL} , Eq. (1).

The optimal entangled state for the HPEA is¹⁵

$$|\psi_{\text{opt}}\rangle = c_0|\Phi^+\rangle + c_1|\Psi^+\rangle, \quad (2)$$

where

$$c_j = \frac{\sin[(j+1)\pi/5]}{\sqrt{\sum_{k=0}^1 \sin^2[(k+1)\pi/5]}}, \quad (3)$$

and where $|\Phi^+\rangle = (|00\rangle + |11\rangle)/\sqrt{2}$ and $|\Psi^+\rangle =$

$(|01\rangle + |10\rangle)/\sqrt{2}$ are Bell states. The optimal adaptive measurement²¹ is implemented by measuring the qubits sequentially in the X basis, and, conditioned on the results, adjusting the controllable phase θ shifts on subsequent qubits, as shown in Fig. 1d.

In our experiment (Fig. 2), we used orthogonal right- and left-circular polarisations instead of paths to form the two arms of the interferometer. We used a nondeterministic CNOT gate, acting on photon polarisation qubits (horizontal $|H\rangle \equiv |0\rangle$, vertical $|V\rangle \equiv |1\rangle$), to generate the state in Eq. (2). As shown in Fig. 1e, the control qubit is prepared in the diagonal polarisation state $|\psi_C\rangle = (|H\rangle + |V\rangle)/\sqrt{2}$, and the target qubit in the linear polarisation $|\psi_T\rangle = c_0|H\rangle + c_1|V\rangle$, so that the output state after the CNOT is the optimal state: $|\psi_{\text{opt}}\rangle = \hat{U}_{\text{CNOT}}(|\psi_C\rangle \otimes |\psi_T\rangle)$. Figure 3 shows the density matrices of the experimentally generated state ρ_{exp} and the ideal state $\rho_{\text{opt}} \equiv |\psi_{\text{opt}}\rangle\langle\psi_{\text{opt}}|$.

The polarisation interferometer, highlighted by the grey background in Fig. 2, used a large half-wave plate (HWP) was used to implement the unknown phase shift between the arms. Mode C was passed twice through this unknown phase. Another HWP (shown in Fig. 2 with a white rim) was used as the reference phase shift θ on mode T, in order to implement the detection scheme.

We implemented the feedforward step nondeterministically, using waveplates that were fixed for each run, combined with postselective sorting of the data based on the results from the detector labeled C. Although this approach would be inadequate for estimation from exactly one shot, it is an accurate way to characterise the performance of the scheme over many repetitions. Table II in Methods shows how the data was sorted and how phase values were allocated for each shot, according to the detector firing patterns. To characterise the performance of our HPEA, we first calculate the condi-

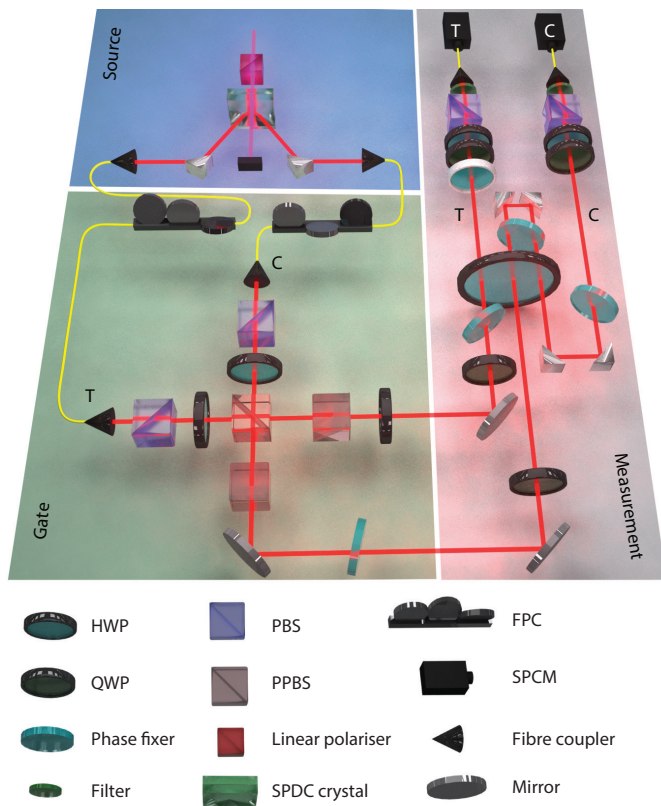


FIG. 2. **Schematic of the experimental setup.** Single photons at 820nm are generated via a type-I spontaneous parametric downconversion (SPDC) process (blue background) and collected using single-mode fibers and pass into the entangling gate (green background) in order to realise the state $|\psi_{\text{exp}}\rangle$. The nondeterministic universal CNOT gate, composed of 3 partially polarising beam splitters (PPBS) and 2 half-wave plates (HWP), performs the state preparation by post-selecting coincidence events between the control and target output ports with success probability $1/9$. The area with gray background corresponds to the implementation of the phase estimation. Photons in mode C pass twice through the HWP (acting as a phase shift element), in order to realise the $U(\phi)^2$ operation. Photons in mode T experience the phase shift once (performing the U operation). The effect of the feedforward operation, $R(\theta)$, is simulated by dialling a HWP (depicted with a white rim), for a fixed time period, in 0 and $\pi/8$ corresponding to the on and off settings of the control operation. Finally, photons are independently directed to a polarisation analysis unit consisting of a quarter-wave plate (QWP), HWP and a polarising beam splitter (PBS) followed by a 2 nm spectral filter and a single photon counting module (SPCM). See Methods for further details on the experimental setup operation.

tional Holevo variance V_H^ϕ in the estimates for each applied phase ϕ (see Methods for details on data analysis). Here $V_H^\phi = |\langle \exp[i(\phi - \phi_{\text{est}})] \rangle_{\phi_{\text{est}}} |^{-2} - 1$ for a given ϕ , where $\langle \dots \rangle_{\phi_{\text{est}}}$ indicates averaging over the values of ϕ_{est} resulting from the data. Figure 4 shows V_H^ϕ for the entire range of $\phi \in [0, 2\pi)$. The protocol performs best

when $\phi = 0, \pi/2, \pi$, and $3\pi/2$, corresponding to the cases where, to a good approximation, only one of the four possible detection outcomes occur: DD , AD , DA , and AA , respectively, as shown in Fig. 1.1. (Here, $D(A)$ means the diagonal (antidiagonal) polarisation states, which are X -basis eigenstates.) It performs worst for intermediate phases. This explains the oscillatory nature of the data in Fig. 4.

Since we are interested in evaluating the precision of *ab-initio* phase estimation, we cannot use any knowledge of ϕ . Thus we erase any initial phase information by calculating the unconditional Holevo variance $V_H = |\langle \langle \exp[i(\phi - \phi_{\text{est}})] \rangle_{\phi_{\text{est}}} \rangle_\phi |^{-2} - 1$, which averages over ϕ . We find $V_H = 0.5497 \pm 0.0007$, whereas the Heisenberg limit for $N = 3$ resources is $V^{\text{HL}} \approx 0.5278$ ²⁵. We attribute this small discrepancy between the experimental result and theoretical bound to the non-unit fidelity of the prepared entangled state with respect to ρ_{opt} , as our numerical simulations of the HPEA, described in Appendix, suggest strong correlation between the protocol performance and quality of the prepared state.

For comparison, we perform standard quantum interferometry with three independent photons (see SI for details). Calculating the Holevo variance for this measurement gives $V_H = 0.7870 \pm 0.0007$ which is close to the theoretical value of $V^{\text{SLN}} = 0.7778$ for the SNL with $N = 3$ resources.

We also compare our results with the theoretically-optimal results for other schemes that use a subset of the three protocol components; see Table I. It can readily be observed that our scheme outperforms all those that use two of the components only. Note that arbitrary entanglement can always do the job of multiple passes, by replacing each multipassed photon with a multiple-photon NOON state⁷, split across the two polarisations. Thus our results could, in principle, be reproduced by an entangled state of three photonic qubits,

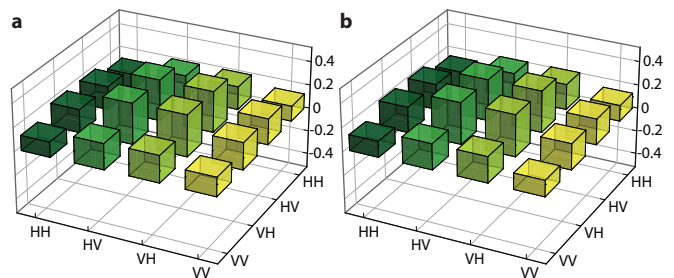


FIG. 3. **Density matrices of the experimental state and ρ_{opt} .** **a**, Real part of the state matrix ρ_{exp} reconstructed with polarisation state tomography. The fidelity of the state with the optimal state $|\psi_{\text{opt}}\rangle$, Eq. (2), is $F = (98.0 \pm 0.3)\%$, and the purity is equal to $P = (96.5 \pm 0.6)\%$. The density matrix was calculated from approximately 50,000 two-fold coincidence events. Uncertainties in F and P represent 95% confidence interval calculated with Monte-Carlo simulation²³. Imaginary components (not shown) are ≤ 0.013 . **b**, Real part of the ideal optimal state ρ_{opt} . $\text{Im}(\rho_{\text{opt}}) = 0$.

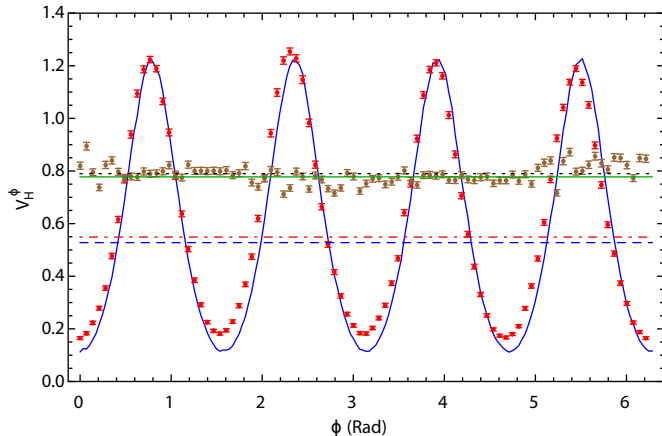


FIG. 4. **Heisenberg-limited phase estimation with $N = 3$ resources.** Red dots represent experimentally measured variance V_H^ϕ as a function of ϕ , and dotted-dashed red line shows the HPEA-protocol Holevo variance $V_H = 0.5497 \pm 0.0007$, determined from these data. The blue curve represents results of numerical simulations of the variance for the ideal optimal state ρ_{opt} . Brown dots represent V_H^ϕ for the shot-noise-limited interferometry and dashed black line represents the measured Holevo variance $V_H = 0.7870 \pm 0.0007$ for the same measurement. Solid green line and dashed blue line show the SNL and the HL, respectively, see Table I. Each data point was calculated from at least 50,000 two-fold coincidence events and the error bars represent 95% confidence interval calculated with the bootstrap method²⁴.

two in one spatio-temporal mode and the third in another, with both modes going through $U(\phi)$ once. We rule out such complicated schemes in our comparison by restricting to symmetric entanglement, in which each photon that passes through $U(\phi)$ a given number of times is prepared identically. (This is the case for the entanglement in our scheme since each of the two photons passes through $U(\phi)$ a different number of times.) We have experimentally demonstrated how to use entanglement, adaptive measurement and multiple passes of the phase shift to perform *ab initio* phase measurement that outperforms any other scheme, in terms of sensitivity per resource. Our results are very close to the Heisenberg limit for $N = 3$, giving substantial experimental justification to the theoretical prediction that this method can saturate the ultimate measurement sensitivity bound. Future work will address realisation of deterministic adaptive measurement using *e.g.* a Pockels cell. Other future extensions to the scheme will employ $K + 1 > 2$ photons, yielding $N = 2^{K+1} - 1$ resources and a correspondingly decreased phase uncertainty, as quantum logic circuits become increasingly capable of producing large entangled states with high fidelity. We note that while we have implemented this scheme optically, it can be applied to the estimation of any parameter that implements a phase shift between qubit states of some physical system.

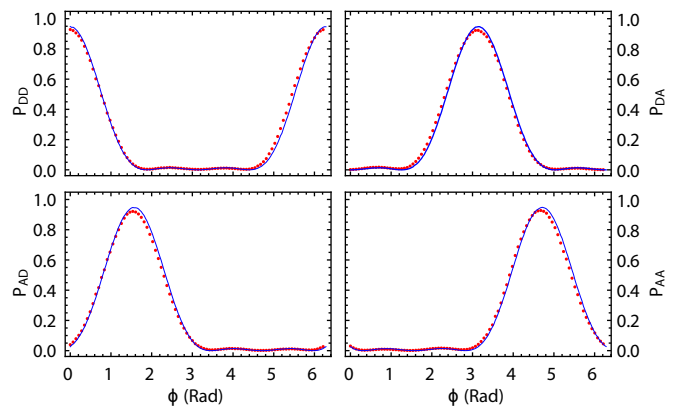


FIG. 5. **Probability distribution of measurement outcomes.** The probabilities of obtaining the four possible $\{DD, DA, AD, AA\}$ measurement outcomes which correspond to four possible ϕ_{est} values. The variance V_H^ϕ is minimised for those ϕ values when one of the probabilities is maximum. Dots are experimental values and lines are numerical simulations that use the parameters of the experimentally generated ρ_{exp} as input. Error bars are smaller than the dot size.

TABLE I. The Holevo variance for different schemes. See SI for derivation of theory results.

Symmetric entanglement	Multipass	Adaptive measurement	V_H
✓	✓	✓	0.5278
✓	✓	✓	0.5497(7) (Exp.)
✓	✗	✓	0.5569 ²⁶
✗	✓	✓	0.5609
✓	✓	✗	0.6546
✗	✗	✗	0.7778
✗	✗	✗	0.7870(7) (Exp.)

METHODS

A. Photon source

We used spontaneous parametric downconversion (SPDC) to produce pairs of polarisation-unentangled single photons. Ultrashort pulses from a mode-locked Ti:sapphire laser at 820 nm with repetition rate of 80 MHz, were downconverted to 410 nm wavelength through a second harmonic generation (SHG) process with a 2 mm Lithium triborate (LBO) crystal. The SHG beam was collimated with a $f = 75$ mm lens and the IR pump was spatially filtered away with two dispersive prisms. The UV light was focused on a 0.5 mm BiBO crystal to generate photon pairs via a type I SPDC. The pump power was set to approximately 100 mW to ensure low probability of double pair emission from the crystal. Using 2 nm narrowband spectral filters, and Excelitas single photon counting modules (SPCMs) with detection efficiency in the range (50-60)%, the coincidence efficiency was in the window of (11 – 13)% with single-detection

count rates of $\sim 40,000$ per second.

B. Entangling gate

The single photons produced in the SPDC process were spatially filtered using antireflection (AR) coated single-mode fibres, and sent through the entangling gate to produce a state close to the optimal state ρ_{opt} . The logical circuit of the gate consisted of three PPBSs, with $\eta_V = 1/3$ and $\eta_H = 1$ for the transmissivity of vertically and horizontally polarised light respectively, to produce a nondeterministic controlled- Z operation²⁷. Two HWPs oriented at 22.5° with respect to the optical axis were used to perform the Hadamard operations required for the correct operation of the CNOT gate. The successful operation of the gate is heralded by the presence of one photon in each output mode of the gate, with overall success probability of $1/9$. At the core of this realisation is the non-classical interference that occurs between vertically polarised photons in mode s C and T impinging on the central PPBS, see Fig. 2. The maximum interference visibility that can be observed with $\eta_V = 1/3$ transmissivity is 80%. We observed $(79 \pm 0.5)\%$ visibility (see Appendix Fig. I.1) Hong-Ou-Mandel interference²⁸, indicating excellent performance of the gate.

C. Encoding phase shifts and realising probabilistic adaptive measurements

To encode both unknown and classically controllable phases we proceeded as follows. The prepared state at the end of the entangling gate is ideally in the form of $|\psi_{\text{opt}}\rangle = c_0|\Phi^+\rangle + c_1|\Psi^+\rangle$, Eq. (2), which is a superposition of the Bell states, $|\Phi^+\rangle = (|HH\rangle + |VV\rangle)/\sqrt{2}$, and $|\Psi^+\rangle = (|HV\rangle + |VH\rangle)/\sqrt{2}$. H and V are horizontal and vertical, respectively, polarisation states of a single photon, and encode the logical 0 and 1 states of a qubit. The linear polarisations were transformed to circular ones prior to the application of the phase shift. This was done by a QWP set at $\pi/4$, yielding

$$\begin{pmatrix} |H\rangle \\ |V\rangle \end{pmatrix} \xrightarrow{U_Q^{(\pi/4)}} \begin{pmatrix} e^{i\pi/4}|R\rangle \\ e^{-i\pi/4}|L\rangle \end{pmatrix}. \quad (4)$$

Here U_Q is the unitary operation for a QWP. The phase shift of ϕ between the right (R) and left (L) circular polarisations could then be applied by setting the 2-inch HWP in Fig. 2 at $-\phi/4 + \pi/8$, producing the transformation

$$\begin{pmatrix} e^{i\pi/4}|R\rangle \\ e^{-i\pi/4}|L\rangle \end{pmatrix} \xrightarrow{U_H^{(-\phi/4 + \pi/8)}} \begin{pmatrix} e^{i\phi}|L\rangle \\ |R\rangle \end{pmatrix}, \quad (5)$$

where we have ignored the global phase factor, and U_H is the matrix for performing HWP operation. Through

TABLE II. The detection outcome patterns.

Outcome in C	θ	Successful events in CT	Rejected events in CT
D	0	DD, DA	AD, AA
A	$\pi/8$	AD, AA	DD, DA

the same procedure we implemented the feedforward operation, but this time the corresponding HWP was set at $\theta/4 + \pi/8$, so that

$$\begin{pmatrix} |H\rangle \\ |V\rangle \end{pmatrix} \xrightarrow{U_Q^{(\pi/4)}} \begin{pmatrix} e^{i\pi/4}|R\rangle \\ e^{-i\pi/4}|L\rangle \end{pmatrix} \xrightarrow{U_H^{(\theta/4 + \pi/8)}} \begin{pmatrix} |L\rangle \\ e^{i\theta}|R\rangle \end{pmatrix}. \quad (6)$$

This way we could encode the phase shift $\phi - \theta$ between the two arms of the interferometer.

The next step was to perform the adaptive measurements, which we implemented in a probabilistic manner. Since the feedback-controlled unitary operation $R(\theta)$ has only two settings in this scheme, we set the corresponding HWP at $\theta = 0$ and collected data for a fixed period of time. We recorded only those coincidence events where detector C (Fig. 2) registered a D -polarised photon, as shown in Table II. We repeated this for $\theta = \pi/8$ and detection of A polarisation at detector C. In other words, when the photon in mode C is projected onto $|D\rangle$ ($|A\rangle$) state, it is expected that the feedforward unit is in an OFF (ON) setting, equivalent to dialling $\theta = 0$ ($\theta = \pi/8$) for the HWP acting on the photon in mode T. This provides for characterisation of the protocol performance without active switching.

Each single shot detection (recorded coincidence) provides $\phi_{\text{est}} = \pi(\phi_0 \times 2^0 + \phi_1 \times 2^1)/2$. Here, $\phi_0\phi_1 \in \{00, 01, 10, 11\} \leftrightarrow \{DD, DA, AD, AA\}$. The probability of obtaining the $\phi_0\phi_1$ result is equal to the number of times $n_{\phi_0\phi_1}$ that this measurement result occurs, divided by the size of the ensemble n_{ens} over which the Holevo variance is calculated. Thus from the measurement record we evaluated the true phase ϕ using the relation

$$\phi \approx \arg \left[\frac{1}{n_{\text{ens}}} \sum_{\phi_0=0}^1 \sum_{\phi_1=0}^1 n_{\phi_0\phi_1} \exp(i\phi_{\text{est}}) \right], \quad (7)$$

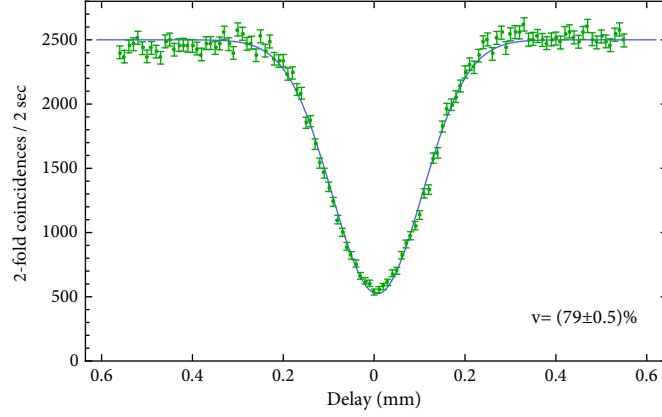
which becomes exact when $n_{\text{ens}} \rightarrow \infty$. The conditional Holevo variance V_H^ϕ is then calculated according to $V_H^\phi = |\langle s \rangle_{\phi_{\text{est}}} |^{-2} - 1$, with $s = \exp[i(\phi - \phi_{\text{est}})]$. Finally, the unconditional Holevo variance^{19,25} is calculated as $V_H = |\langle s \rangle_{\phi_{\text{est}}, \phi} |^{-2} - 1$.

- [1] Berry, D. W., & Wiseman, H. M. Optimal States and Almost Optimal Adaptive Measurements for Quantum Interferometry. *Phys. Rev. Lett.* **85**, 5098-5101 (2000).
- [2] Higgins, B. L., Berry, D. W., Bartlett, S. D., Wiseman, H. M., & Pryde, G. J. Entanglement-free Heisenberg-limited phase estimation. *Nature* **450**, 393-396 (2007)
- [3] Wiseman, H. M., & Milburn, G. J. Quantum Measurement and Control (Cambridge Univ. Press, 2010).
- [4] Giovannetti, V., Lloyd, S., & Maccone, L. Quantum metrology. *Phys. Rev. Lett.* **96**, 010401 (2006).
- [5] Caves, C. M. Quantum-mechanical noise in an interferometer. *Phys. Rev. D* **23**, 1693 (1981).
- [6] Giovannetti, V., Lloyd, S., & Maccone, L. Advances in quantum metrology. *Nat. Photon.* **5**, 222-229 (2011)
- [7] Dowling, J. P. Quantum optical metrology – the lowdown on high-NOON states. *Contemp. Phys.* **49**, 125143 (2008)
- [8] Nagata, T., Okamoto, R., O’Brien, J. L., Sasaki, K., & Takeuchi, S. Beating the Standard Quantum Limit with Four-Entangled Photons. *Science* **316**, 726-729 (2007)
- [9] Slussarenko, S., Weston, M. M., Chrzanowski, H. M., Shalm, L. K., Verma, V. B., Nam, S. W., & Pryde, G. J. Unconditional violation of the shot noise limit in photonic quantum metrology. *Nat. Photon.* **11**, 700-703 (2017)
- [10] Moreau, P.-A., Sabines-Chesterking, J., Whittaker, R., Joshi, S. K., Birchall, P. M., McMillan, A., Rarity, J. G., & Matthews, J. C. F. Demonstrating an absolute quantum advantage in direct absorption measurement. *Sci. Rep.* **7**, 6256 (2017)
- [11] Sabines-Chesterking, J., Whittaker, R., Joshi, S. K., Birchall, P. M., Moreau, P. A., McMillan, A., Cable, H. V., O’Brien, J. L., Rarity, J. G., & Matthews, J. C. F. Sub-Shot-Noise Transmission Measurement Enabled by Active Feed-Forward of Heralded Single Photons. *Phys. Rev. Applied* **8**, 014016 (2017)
- [12] Xiang, G. Y., Higgins, B. L., Berry, D. W., Wiseman, H. M., & Pryde, G. J. Entanglement-enhanced measurement of a completely unknown optical phase. *Nat. Photon.* **5**, 43-47 (2011)
- [13] Berni, A. A., Gehring, T., Nielsen, B. M., Händchen, Paris, H. M. G. A., & Andersen, U. L. Ab initio quantum-enhanced optical phase estimation using real-time feedback control. *Nature Photon.* **9**, 577-581 (2015)
- [14] Holevo, A. S. Covariant measurements and imprimitivity systems. *Lect. Notes Math.* **1055**, 153-172, (1984)
- [15] Wiseman, H. M., Berry, D. W., Bartlett, S. D., Higgins, B. L., & G. J. Pryde Adaptive measurements in the optical quantum information laboratory. *IEEE J. Sel. Top. Quantum Electron.* **15**, 1661-1672 (2009).
- [16] Waldherr, G., and Beck, J., Neumann, P., Said, R. S., Nitsche, M. Markham, M. L., Twitchen, D. J., Twamley, J., Jelezko, F., & Wrachtrup, J. High-dynamic-range magnetometry with a single nuclear spin in diamond. *Nat. Nanotech.* **7**, 105-108 (2012)
- [17] Nusran, N. M., Ummal Momeen, M., & Gurudev Dutt, M. V High-dynamic-range magnetometry with a single electronic spin in diamond. *Nat. Nanotech.* **7**, 109-113 (2012)
- [18] Berry, D. W., & Wiseman, H. M. Optimal States and Almost Optimal Adaptive Measurements for Quantum Interferometry. *Phys. Rev. Lett.* **85**, 5098-5101 (2000).
- [19] Berry, D. W., Wiseman, H. M., & Breslin, J. K. Optimal input states and feedback for interferometric phase estimation. *Phys. Rev. A* **63**, 053804 (2001).
- [20] Sanders, B. C., & Milburn, G. J. Optimal Quantum Measurements for Phase Estimation. *Phys. Rev. Lett.* **75**, 2944-2947 (1995).
- [21] Griffiths, R. B., & Niu, C. Semiclassical Fourier Transform for Quantum Computation. *Phys. Rev. Lett.* **76**, 3228 (1996).
- [22] Nielsen, M. A., & Chuang, I. L. Quantum Computation and Quantum Information (Cambridge Univ. Press, 2001).
- [23] White, A. G., Gilchrist, A., Pryde, G. J., O’Brien, J. L., Bremner, M. J., & Langford N. K. Measuring two-qubit gates. *J. Opt. Soc. Am. B* **24**, 172-183 (2007)
- [24] Davidson, A. C., and Hinkley, D. V. Bootstrap methods and their application (Cambridge Univ. Press, 2010).
- [25] Berry, D. W., Higgins, B. L., Bartlett, S. D., Mitchell, M. D., Pryde, G. J., & Wiseman, H. M. How to perform the most accurate possible phase measurements. *Phys. Rev. A* **80**, 052114 (2009).
- [26] D. W. Berry, Adaptive Phase Measurements, PhD Thesis, The University of Queensland, 2001; arXiv:quant-ph/0202136.
- [27] Ralph, T. C. & Pryde, G. J. Optical quantum computation. *Prog. Opt.* **54**. 209-269 (2009).
- [28] Hong, C. K., Ou, Z. Y., & Mandel, L. Measurement of subpicosecond time intervals between two photons by interference. *Phys. Rev. Lett.* **59** 2044 (1987).

ACKNOWLEDGEMENT

The authors thank R. B. Patel for assistance with data acquisition code. S. D. acknowledges financial support by the Australian Government Research Training Program Scholarship. This research was supported by the Australian Research Council Centre of Excellence Grant No. CE110001027. D.W.B. is funded by an Australian Research Council Discovery Project Grant No. DP160102426.

I. APPENDIX



Appendix Figure I.1. **Hong-Ou-Mandel interference at the CNOT gate.**

A. Numerical simulation of the HPEA

Consider the Heisenberg-limited interferometric phase estimation algorithm with $K + 1 = 2$ (qubits) photons shown in Fig. 1d. Assume the input state is represented by ρ_{in} which allows us to consider mixed input states. The state $\rho^{(K)} \in \mathbb{B}_{2^{K+1}}$ (\mathbb{B} denoting Banach space) of the system before the first X -measurement on the K -th photon is

$$\rho^{(K)} = \left(U^{2^K} \bigotimes_{k=1}^K \hat{I} \right) \rho_{\text{in}} \left(U^{2^K} \bigotimes_{k=1}^K \hat{I} \right)^\dagger, \quad (\text{S1})$$

where

$$U^p = \begin{pmatrix} 1 & 0 \\ 0 & e^{ip\phi} \end{pmatrix}, \quad \hat{I} = \begin{pmatrix} 1 & 0 \\ 0 & 1 \end{pmatrix}. \quad (\text{S2})$$

Here ϕ is a random unknown phase in the interval $[0, 2\pi)$ to be estimated. To find the outcome of the X -measurement on the K -th photon, we define the following two measurement operators

$$\hat{M}_r^{(K)} = \hat{P}_r \bigotimes_{k=1}^K \hat{I}, \quad (\text{S3})$$

where $r = (D, A)$ is a measurement result, and $\hat{P}_r = |r\rangle\langle r|$ is the projection operator onto the X basis of the K -th photon. Thus, the probability of finding the K -th photon in one of the X eigenstates is

$$p_r^{(K)} = \text{Tr} \left[\rho^{(K)} \hat{M}_r^{(K)} \hat{M}_r^{(K)\dagger} \right] = \text{Tr} \left[\rho^{(K)} \hat{M}_r^{(K)} \right]. \quad (\text{S4})$$

Whether the K -th qubit is found in $|D\rangle$ or $|A\rangle$ is determined by calling a random number and comparing it with the above probability. Depending on the outcome of this last step, the conditional system state $\rho_r^{(K)}$ after the measurement on the K -th photon is obtained according to³

$$\rho_r^{(K)} = \mathcal{J} \left[\hat{M}_r^{(K)} \right] \rho^{(K)} / p_r^{(K)} = \hat{P}_r \otimes \rho_r^{(K-1)}, \quad (\text{S5})$$

where $\rho_r^{(K-1)} \in \mathbb{B}_{2^K}$ is the reduced state matrix of the other remaining K photons. Here $\mathcal{J}[\hat{O}]\hat{A} \equiv \hat{O}\hat{A}\hat{O}^\dagger$ for some arbitrary operators \hat{O} and \hat{A} . To proceed with the next step of the protocol, the result of the previous measurement is used to decide whether feedforward should be applied or not. That is, the outcomes $r = A$ and $r = D$ correspond to

control operation ‘‘ON’’ and ‘‘OFF’’, respectively. Therefore, in the reduced-dimension Hilbert space of the system, the state matrix before the measurement on the $(K-1)$ -th photon when the feedback operation is ON can be expressed as

$$\rho^{(K-1)} = V^{(K-1)} \rho_r^{(K-1)} V^{(K-1)\dagger}, \quad (\text{S6})$$

where

$$V^{(K-1)} \equiv \left[U^{2^{K-1}} R\left(\frac{\pi}{2}\right) \right] \bigotimes_{k=2}^K R\left(\frac{\pi}{2^k}\right), \quad (\text{S7})$$

$$R(\theta) = \begin{pmatrix} e^{i\theta} & 0 \\ 0 & 1 \end{pmatrix}, \quad (\text{S8})$$

and if the feedforward is OFF, the state matrix is

$$\rho^{(K-1)} = \left(U^{2^{K-1}} \bigotimes_{k=1}^K \hat{I} \right) \rho_r^{(K-1)} \left(U^{2^{K-1}} \bigotimes_{k=1}^K \hat{I} \right)^\dagger. \quad (\text{S9})$$

Measurement on the $(K-1)$ -th photon is described in the same way as that of the K -th photon. That is, by changing $K \rightarrow K-1$ we can use Eqs. (S3)–(S9) to find the measurement result and the reduced state $\rho_r^{(K-2)} \in \mathbb{B}_{2^{K-1}}$ of the system. These steps are repeated for each qubit until the 0-th one, for which, the measurement operator is simply the projector $\hat{M}_r^{(0)} = \hat{P}_r$. Finally the same procedure as described in Methods is employed to calculate the Holevo variance.

B. Shot Noise Limit: analytical calculation

The asymptotic limit of the phase variance can be calculated in an interferometric phase estimation context to obtain the SNL which amounts to $V^{\text{SNL}} \sim 1/N$. This limit is valid when the number N of resources goes to infinity. When N is finite and small, as is the case here in our experiment, this relation does not hold at all. Instead, we were required to analytically calculate what is the SNL for small N 's²⁵.

Consider the interferometer shown in Fig. 1a without multipassing, that is, $p = 1$. Sending single-photon Fock state into one arm of the interferometer, the probability of detecting a photon in either of the output ports in an ideal experimental situation is given by

$$P(u|\phi, \theta) = \frac{1}{2} [1 + u \cos(\phi - \theta)], \quad (\text{S10})$$

where $u \in \{-1, 1\}$ labels the measurement outcome. Assuming that N measurement results are obtained, we can represent them as a vector $\mathbf{u}_N = (u_1, u_2, \dots, u_N)$ in which each u_j is defined as above. Therefore, the probability for the sequence of measurement results is given by

$$P(\mathbf{u}_N|\phi, \boldsymbol{\theta}) = P(u_1|\phi, \theta_1) P(u_2|\phi, \theta_2) \cdots P(u_N|\phi, \theta_N), \quad (\text{S11})$$

where the adjustable phase is varied according to $\theta_j = j\pi/N$. Now recall the Holevo variance in the phase estimate $V_H = \mu^{-2} - 1$ where the sharpness $\mu = |\langle e^{i\phi} \rangle|$. Using the conditional probability given in Eq. (S11), μ can be written as^{19,25}

$$\mu = \frac{1}{2\pi} \sum_{\mathbf{u}_N} \left| \int e^{i\phi} P(\mathbf{u}_N|\phi, \boldsymbol{\theta}) d\phi \right|. \quad (\text{S12})$$

We can then calculate the Holevo variance for small N 's by solving this integral. For our experiment in which $N = 3$, we could easily calculate the sharpness and find the exact standard quantum limit to be $V^{\text{SNL}} = 7/9$. However, as the number of resources increases this calculation gets complex and at some point even impossible to solve the integral exactly as the number of possible results goes up exponentially.

C. Shot Noise Limit: experiment

To measure the SNL we have used the same experimental setup. Unentangled single photons were guided through the interferometer such that one of them was used as a probe system and the other one heralded the presence of the former. Instead of passing three photons once through the phase shift element, we sent three single photons sequentially one after the other and adjusted the controllable phase to θ_j , respectively, for $j = 1, 2$, and 3 . For each setting there would be two measurement outcomes u_j . This means for a fixed ϕ there are $2^3 = 8$ possible results (two of which, $\phi_1 = \phi_3 = \pm 1$ and $\phi_2 = \mp 1$, are not useful because they yield no information about the unknown phase). Let $n_{u_j}(\phi, \theta_j)$ represents the number of times that a particular outcome turns up out of an ensemble size $n_{\text{ens}} = \sum_{u_j} n_{u_j}(\phi, \theta_j)$. Therefore, the probability of having the outcome $\mathbf{u}_3 = (u_1, u_2, u_3)$ for three independent measurement is

$$P(\mathbf{u}_3|\phi) = \prod_j \frac{n_{u_j}(\phi, \theta_j)}{n_{\text{ens}}}, \quad (\text{S13})$$

and the true phase can be calculated using

$$\phi = \arg \sum_{\mathbf{u}_3} \int P(\mathbf{u}_3|\phi) e^{i\phi} d\phi. \quad (\text{S14})$$

On the other hand, ϕ_{est} for three measurement outcomes \mathbf{u}_3 is

$$\phi_{\text{est}}(\mathbf{u}_3) = \arg \int \prod_j P(u_j|\phi, \theta_j) e^{i\phi} d\phi. \quad (\text{S15})$$

For a given ϕ we proceeded as the following to calculate the sharpness

$$\mu(\phi) = \left| \sum_{\mathbf{u}_3} P(\mathbf{u}_3|\phi) e^{i(\phi - \phi_{\text{est}})} \right|. \quad (\text{S16})$$

It is easy to work out the Holevo variance by averaging over ϕ in the same way as before.

D. Holevo variance for the protocols in Table I

For the case of adaptive measurements and entanglement but no multiple passes, we consider 3 photons in a single spatio-temporal mode so they are indistinguishable. That is, by construction, the photons are identically prepared; the entanglement is symmetric under photon exchange. This single mode could be over an extended time, so photons can be detected separately, and the controlled phase can be adjusted in between detections. As discussed in the main text, if we had instead considered three distinguishable photons in different modes, then having entanglement and adaptive measurements would be the most powerful scheme possible, and would give the same Holevo variance as using symmetric entanglement, multiple passes and adaptive measurements.

There are a total of 3 phases that need to be optimised. Before the first detection, the controllable phase θ has no effect on the results. This is because the system phase is averaged over, and it is only the relative phases that are important. There are two possibilities for the first detection result, and values of the controllable phase θ need to be chosen for each. There are four possibilities for the first two detection results, and again values of the controllable phase θ after those two detections need to be chosen. This gives six phases, but changing the initial value of ϕ by π reverses the significance of the detection results. Because of this symmetry the number of phases that need be considered is reduced by a factor of 2. In addition, the entangled state needs to be optimised over.

Results for the case where the state is optimal for canonical measurements were given in Fig. 11 of Ref.¹⁹, where it was found that the phase variance was slightly above that for canonical measurements for 3 photons. That result shows that it is not possible to achieve the HL in that case, though it leaves open the possibility that slightly better performance (but still not at the HL) could be obtained by optimising over the state as well. The result for that case was given in Fig. 6.10 of Ref.²⁶, and the optimisation over the state gives a very slight improvement for $N = 3$. The exact value obtained was 0.5569202271898053.

For the case with adaptive measurements and multiple passes but no entanglement, there are three general possibilities for $N = 3$.

1. One photon with three passes.

2. One photon with two passes and one photons with one pass.
3. Three single photons with a single pass each.

The first is trivial because there is phase ambiguity so the Holevo variance is infinite. The second can be treated using the approach of Sec. IV of Ref.²⁵, where an equivalent two-mode state in a single time mode is considered. There it was found that the ideal canonical measurement gives a variance of $2/N + 1/N^2$ (see Eq. (4.4)). For $N = 3$ this gives $7/9 = 0.777\dots$. A result for the third possibility was given in Fig. 6.7 of Ref.²⁶, though with a restricted optimisation of the adaptive measurements, and obtained a Holevo variance of 0.5609756097560981. We have recalculated the variance with full optimisation over θ , and found that the variance is unchanged.

Finally we consider the case of symmetric entanglement and multiple passes, but no adaptive measurements. There are three possibilities again, and again the case with one photon and three passes is trivial. For the others, it is necessary to optimise over the controlled phases θ and the state. The optimisation over the phases is simpler than for the adaptive case, because the phase does not depend on the detection results. It was found that for one photon with two passes and another with a single pass the minimum Holevo variance was 2. The best result was for three entangled photons in a single mode and single passes, in which case the minimum Holevo variance was 0.6546809936433506. We note that if one were to drop the requirement of symmetry on the entangled state, one could obtain a slightly smaller variance of 0.6054864794870138, using an entangled state across three modes.

These calculations were performed in the following way. First, a state of three successive photons in different spatio-temporal modes can be given as

$$|\psi\rangle = \sum_{j,k,l \in \{0,1\}} \psi_{j,k,l} |j, k, l\rangle, \quad (\text{S17})$$

where j , k , and l indicate which polarisation each photon is in. This formalism can also be used to treat multiple photons in the same spatio-temporal mode, by using a symmetric state.

Then the operation of measuring a photon as being in one polarisation or the other on the first mode can be represented by

$$\langle a|\psi\rangle = \sum_{j,k,l \in \{0,1\}} \psi_{j,k,l} \langle a|j\rangle |k, l\rangle, \quad (\text{S18})$$

where

$$|a\rangle = \frac{1}{\sqrt{2}}(|0\rangle + (-1)^a|1\rangle), \quad (\text{S19})$$

for $a \in \{0, 1\}$. It is easy to see that

$$\langle a|j\rangle = \frac{1}{\sqrt{2}}(-1)^{aj}. \quad (\text{S20})$$

For three measurement results, a , b , and c , the inner product we need is

$$\begin{aligned} \langle a, b, c|\psi\rangle &= \sum_{j,k,l \in \{0,1\}} \psi_{j,k,l} \langle a|j\rangle \langle b|k\rangle \langle c|l\rangle \\ &= \sum_{j,k,l \in \{0,1\}} \psi_{j,k,l} (-1)^{aj+bk+cl} \end{aligned} \quad (\text{S21})$$

Similarly to how described in previous sections, the probability of obtaining the measurement result is given by the absolute value squared:

$$P(a, b, c) = |\langle a, b, c|\psi\rangle|^2. \quad (\text{S22})$$

Next we explain how to take the phase into consideration. Without loss of generality we can take the first controlled phase θ_0 to be zero (since we average over ϕ). The second controlled phase θ_1 can depend on a , and the third θ_2 can depend on a and b . The change in the state with these controlled phases and the system phase ϕ is

$$|\psi(\phi)\rangle = \sum_{j,k,l \in \{0,1\}} e^{i[j\phi+k(\phi-\theta_1)+l(\phi-\theta_2)]} \psi_{j,k,l} |j, k, l\rangle. \quad (\text{S23})$$

This state is convenient to use for calculation, but will not correspond to the physical state at any stage. In reality the first photon would be detected before the phase $\phi - \theta_1$ is applied to the second photon, and so forth. The important quantity is the inner product

$$\langle a, b, c | \psi(\phi) \rangle = \sum_{j,k,l \in \{0,1\}} e^{i[j\phi + k(\phi - \theta_1) + l(\phi - \theta_2)]} (-1)^{aj + bk + cl} \psi_{j,k,l} \quad (\text{S24})$$

which enables us to calculate the probability as a function of ϕ

$$P(a, b, c | \phi) = |\langle a, b, c | \psi(\phi) \rangle|^2. \quad (\text{S25})$$

Next, we determine the Holevo variance with sharpness μ given by

$$\mu = \frac{1}{2\pi} \sum_{a,b,c \in \{0,1\}} \left| \int e^{i\phi} P(a, b, c | \phi) d\phi \right|. \quad (\text{S26})$$

We can calculate the integral as

$$\int e^{i\phi} P(a, b, c | \phi) d\phi = \sum_{j+k+l+1=j'+k'+l'} e^{i[(j-j')\phi + (k-k')(\phi - \theta_1) + (l-l')(\phi - \theta_2)]} (-1)^{a(j-j') + b(k-k') + c(l-l')} \psi_{j,k,l} \psi_{j',k',l'}^*. \quad (\text{S27})$$

This formula can be used to minimise the phase variance with various types of measurement. If the measurement is allowed to be adaptive, then θ_1 can depend on a and θ_2 can depend on a and b . If it is not adaptive, then θ_1 and θ_2 would need to be chosen independently of the measurement results. Restrictions on the state can also be imposed, for example by requiring it to be separable between the three modes, or by requiring it to be symmetric between the three photons to correspond to three photons in the one mode.